Available online at www.sciencedirect.com
ScienceDirect
Trans. Nonferrous Met. Soc. China 33(2023) 1214−1232
Transactions of Nonferrous Metals Society of China
www.tnmsc.cn

A review on theory, modeling, inversion, and application of self-potential in marine mineral exploration

Jing XIE[1,2,3], Yi-an CUI[1,2,3], Jian-xin LIU[1,2,3], You-jun GUO[1,2,3], Li-juan ZHANG[1,2,3], Yi-jian LUO[1,2,3], Peng-fei ZHANG[1,2,3]

1. School of Geosciences and Info-physics, Central South University, Changsha 410083, China;
2. Hunan Key Laboratory of Nonferrous Resources and Geological Disaster Exploration, Changsha 410083, China;
3. Key Laboratory of Metalorganic Prediction of Nonferrous Metals and Geological Environment Monitoring, Ministry of Education, Central South University, Changsha 410083, China

Received 25 October 2021; accepted 16 March 2022

Abstract: The self-potential (SP) method is one of the passive geophysical exploration techniques, which employs measurements of naturally occurring electric potential differences on the ground surface and in boreholes or (sea-)water due to causative sources from electrochemical, electrokinetic, and thermoelectric mechanisms. SP signals are directly related to groundwater flow and (electro-)chemical gradient. There has been increasing interest in the application of SP measurements in mineral exploration, environmental surveys, and hydrogeophysical problems. This review focuses primarily on the theory concerning the causative source mechanism, numerical modeling, and inversion and interpretation of SP signals related to ore bodies and applications in mineral exploration. Three field examples focusing on seafloor sulfide deposits exploration are summarized to show the application effect of SP measurements in marine mineral exploration. This study would be helpful to investigating the use of SP surveys in ore prospecting, especially in marine environments.

Key words: self-potential; marine mineral exploration; source mechanism; numerical modeling; inversion and interpretation

1 Introduction

The self-potential (or spontaneous polarization) (SP) method is a passive geophysical method, which employs measurements of the electrical potential distribution triggered by one or more electrochemical, electrokinetic, and thermoelectric gradients on the ground surface and in boreholes or (sea-)water [1]. SP measurements typically aim to locate or delineate the potential sources pertaining to these causative mechanisms. As one of the oldest geophysical techniques, field SP measurements extend back nearly 200 years, when FOX [2] first investigated SP anomalies associated with sulfide deposits. However, the common use of the fast, inexpensive, and non-intrusive method dated from the 1920s when the use of non-polarized electrode that is the indispensable equipment for SP measurements was introduced [3]. Due to the distinct advantages that the SP method requires simple instrumentation, and SP signals are directly related to the process of interest, such as changes in fluid flow, chemistry and temperature [3], there has been increasing interest in applying SP surveys in many geophysical, geochemical, biogeophysical, biogeochemical, hydrogeological, and hydro-geophysical problems [1].

Corresponding author: Yi-an CUI, Tel: +86-13975894892, E-mail: cuiyian@csu.edu.cn
DOI: 10.1016/S1003-6326(23)66177-1

There are three generally accepted SP current source mechanisms, i.e., electrochemical, electrokinetic, and thermoelectric forces. The electrochemical origin is typically associated with diffusion, exclusion and redox processes, and the latter is the main component in field surveys. SP signals from oxidation−reduction have two contributions. One is contributed from the half-cell reactions related to ore bodies [4], the other is from redox reactions where bacteria participate in the process of SP generation (usually observed at organic-rich contaminated sites) [5]. The major application of the former redox process exists in mineral exploration, and in both on-land and marine environments. In order to qualitatively explain SP anomalies associated with ore bodies, SATO and MOONEY [4] introduced a pathbreaking concept of "geobattery" on the electrochemical mechanism. The geobattery model suggests that surface SP measurements usually show negative electric potential anomalies induced by redox processes occurring on the surface of ore bodies, which helps to delineate the potential area of ore bodies. The early applications are mainly in on-land environments such as prospecting of copper-polymetallic [6], pyrite [7], sulfide [8], graphite [9], and gold [10,11] deposits. Some lab-based experiments also provide evidence favoring the geobattery model. For example, CASTERMANT et al [12] and RITTGERS et al [13] observed SP anomalies in laboratory experiments that aim to monitor the corrosion of buried metallic objects, during which the whole system acts as a small-scale geobattery. After the first attempt in marine mineral exploration by CORWIN [14] who conducted a measurement with an offshore SP array towed behind a small boat and recorded an anomaly of up to 300 mV, the SP method has attracted a lot of interest in marine prospecting for seafloor massive sulfide (SMS) deposits [15−29]. For instance, BELTENEV et al [20−22] conducted the SP measurements, combined with other surveys like temperature and conductivity surveys, geological sampling, near-bottom side-scan sonar, etc., and aimed to investigate indicators associated with recent or extinct hydrothermal activity and related mineralization within the Mid-Atlantic Ridge. SAFIPOUR et al [23] carried out an SP test at the Palinuro Seamount in the Tyrrhenian Sea, where SMS deposits have been proven to exist by MINNITI and BONAVIA [30] and PETERSEN et al [31]. KAWADA and KASAYA [24] performed an SP survey in the hydrothermal field, the Izena hole in the Mid-Okinawa Trough, where a known Kuroko-type SMS deposit exists [32,33]. KAWADA and KASAYA [25], CONSTABLE et al [26], and KASAYA et al [27] also performed marine SP measurements using autonomous underwater vehicles to explore SMS deposits in hydrothermal fields. For the second redox process, the major application of SP measurements contributes to delineating or monitoring organic-rich contaminant plumes [34−39] and dense/light non-aqueous phase liquids [40−42]. The above applications suggest that electrochemical mechanisms mainly contribute to mineral exploration and environmental surveys.

Another causative source, contributed by the electrokinetic phenomenon, can generate the attendant electric potential anomaly, known as the streaming (or electrokinetic) potential. This SP signal has a direct correlation with the movement of underground fluids, during which the hydraulic gradient drags the excess positive charges in the capillary diffusion layer, causing more positive charges to accumulate in the direction of the flow and negative charges upstream, thus forming a measurable electric field [43]. Streaming potential anomalies help to address some engineering, environmental, hydrogeological, and (hydro-)-geophysical problems, including estimating Darcy velocity [44], monitoring earthquakes [45], detecting leakages of dams or embankments [46,47], monitoring pumping tests [48], determining water table [49], indicating groundwater flow [50], characterizing infiltration or evaporation processes [51], and investigating seawater intrusion (coupled with the diffusion potential induced by ion concentration differences) [52]. In addition, the SP signal triggered by the thermoelectric mechanism is mainly contributed by the temperature gradient and is appropriate for limited scenarios such as investigating volcanic and geothermal activity [53,54] and locating coal fires [55]. Since subsurface temperature gradients usually involve fluid circulation, such as in terrestrial geothermal zones and submarine hydrothermal systems, thermoelectric mechanisms are often accompanied by electrokinetic mechanisms.

This paper focuses primarily on reviewing the relevant work of the SP method concerning the theory of causative source mechanisms, numerical modeling, inversion and interpretation, and applications in marine mineral exploration. The theory including three mechanisms of SP sources and the introduction to SP measurements are given in Section 2. Section 3 describes the methodology for simulation or forward modeling, and inversion and interpretation algorithms mainly related to mineral exploration. Section 4 provides a detailed introduction to the use of the SP method in mineral exploration and three marine prospecting cases. The discussion and conclusion are placed in the last two sections.

2 Theory

2.1 Poisson equation

The underground charge polarization mechanism causing SP anomalies can be derived from a variety of sources. SP signals play a role in maintaining overall electroneutrality when charges separate under natural or induced gradients [56,57]. At the macroscopic scale, the coupling conduction phenomenon assumes that SP currents are linearly correlated with causative mechanisms, and the linear coupling equation can be written as [58−60]

$$\begin{bmatrix} \Gamma_1 \\ \Gamma_2 \\ \Gamma_3 \\ \Gamma_4 \end{bmatrix} = \begin{bmatrix} L_{11} & L_{12} & L_{13} & L_{14} \\ L_{21} & L_{22} & L_{23} & L_{24} \\ L_{31} & L_{32} & L_{33} & L_{34} \\ L_{41} & L_{42} & L_{43} & L_{44} \end{bmatrix} \begin{bmatrix} X_1 \\ X_2 \\ X_3 \\ X_4 \end{bmatrix} \tag{1}$$

where Γ_i is the flux (charge, matter, heat, etc.), X_j is the force (gradients of electric potentials, pressures, temperature, etc.), and L_{ij} is the coupling coefficient.

These forces and resulting fluxes include electric potential differences and current densities (i.e., Ohm's law), pressure gradients and fluid velocities (i.e., Darcy's law), chemical gradients and solute fluxes (i.e., Fick's law), and heat gradients and heat fluxes (i.e., Fourier's law) [60]. The total current density $\boldsymbol{J}$ (A·m^{-2}) consists of the forces, thus can be expressed as

$$\boldsymbol{J}=\boldsymbol{J}_{\mathrm{c}}+\boldsymbol{J}_{\mathrm{k}}+\boldsymbol{J}_{\mathrm{e}}+\boldsymbol{J}_{\mathrm{t}} \tag{2}$$

where $\boldsymbol{J}_{\mathrm{c}}$ is the conduction-current density, $\boldsymbol{J}_{\mathrm{k}}$, $\boldsymbol{J}_{\mathrm{e}}$ and $\boldsymbol{J}_{\mathrm{t}}$ are current density contributions from electrokinetic, electrochemical, and thermoelectric origins, respectively (A·m^{-2}). Equation (2) shows that the total current density $\boldsymbol{J}$ equals the conduction-current density $\boldsymbol{J}_{\mathrm{c}}$ conforming to the Ohm's law ($\boldsymbol{J}_{\mathrm{c}}=-\sigma\nabla\varphi$) plus the SP current density $\boldsymbol{J}_{\mathrm{SP}}$ ($\boldsymbol{J}_{\mathrm{SP}}=\boldsymbol{J}_{\mathrm{k}}+\boldsymbol{J}_{\mathrm{e}}+\boldsymbol{J}_{\mathrm{t}}$):

$$\boldsymbol{J}=-\sigma\nabla\varphi+\boldsymbol{J}_{\mathrm{SP}} \tag{3}$$

where σ is the electric conductivity (S·m^{-1}), and φ is the electric potential (V). Charge conservation, in the absence of external sources or sinks, should be such that the divergence equals zero ($\nabla\cdot\boldsymbol{J}=0$), thus resulting in the Poisson equation governing SP signals:

$$\nabla\cdot\sigma\nabla\varphi=\nabla\cdot\boldsymbol{J}_{\mathrm{SP}} \tag{4}$$

2.2 Charge polarization mechanism

2.2.1 SP from electrochemical origin

The SP anomaly from electrochemical origins occurs when the charge transport responds to changes in chemical potentials. In the subsurface, changes in chemical gradients may be caused by changes in the concentration of salt species in the water occupying the pore space or variations in redox potentials related to, for example, variations in oxygen fugacity or pH, and/or bacterial activities. These two electrochemical contributions to SP signals are associated with two types of charge carriers, i.e., ions and electrons [5]. The latter is of more interest to field work such as mineral exploration and environmental surveys. Here, we focus mainly on the SP signal triggered through the redox process related to ore bodies.

Electron transport: SP anomalies related to redox processes are often large, reaching several tens or hundreds of mV over ore bodies [61], buried metallic objects [12,13], and organic-rich contaminant plumes [5,34−39]. In the former two cases, the path for electron transport is clear, i.e., the electrically conductive ore bodies or metallic objects [4,12,13,62]. For the latter, the transport route for electrons is less obvious. Potential electronic conduction paths may result from (1) bacteria and (semi-)conductive minerals being involved in facilitating electron transfer, (2) bacterial colonies forming a network of nanowires through conductive pili, and (3) electrons being transferred from donors to acceptors via insulated wires inside the filamentous bacteria [5,63−66].

Geobattery model: The geobattery model

proposed by SATO and MOONEY [4] suggests that an oxidized zone is formed in the shallow layer due to the infiltration of rainwater and the diffusion of oxygen, a reduction zone is formed at depth, and conductive minerals connect such oxidized and reduction zones and transfer electrons upward. The upper part of the conductive mineral, as a result, releases electrons to form a cathode of the geobattery (e.g., O_2 is reduced as an electron acceptor), and the lower part gains electrons to form an anode of the geobattery (e.g., Fe^{2+} is oxidized as an electron donor). In on-land environments, the two electrochemical half-cell reactions in the geobattery model occur above and below the water table, and the water table acts as the redox boundary. In the marine environment, SP signals also can be explained by the geobattery model. The presence of fluid circulation around ore bodies introduces oxic seawater that strengthens the redox boundary below the seafloor. It should be noted that whether the redox boundary lies below the seafloor depends on the presence or absence of seafloor water circulation. In the former case, the redox boundary is located below the seafloor, and the seafloor itself acts as a redox boundary in the latter condition [24,25]. A sketch of a natural geobattery in both on-land and marine environments is given in Fig. 1.

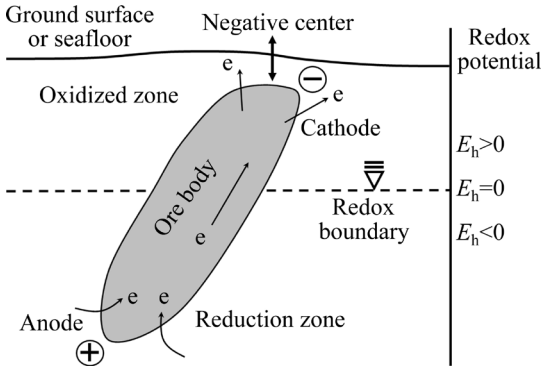

Fig. 1 Geobattery model in on-land or marine environments (Redrawn from Refs. [4,5,12,67])

SP from ore body: To quantitatively interpret SP signals related to the inert ore bodies, STOLL et al [62] and BIGALKE and GRABNER [68] developed a numerical model for calculating the SP current source triggered by redox gradients. Such a model not only explains the E_h gradient with depth predicted by SATO and MOONEY [4] but also includes the electrode kinetics on the mineral surface. At the ore−water interface, the conduction mechanism changes from electronic to electrolytic conduction. The current exchange density represents the source density for the ionic current within the groundwater. The SP current density in Eq. (4) becomes [62,68]

$$\boldsymbol{J}_{SP} = -\boldsymbol{J}_{eh}\frac{nF}{RT}(E_h - E_m + \varphi) \tag{5}$$

where $\boldsymbol{J}_{eh}$ is the exchange current density ($A\cdot m^{-2}$), which is zero everywhere except on the surface of the ore body, E_h is the subsurface redox potential over depth (V), E_m is the electrode potential of the ore body (V), and n, F, R and T are, the number of molar equivalents, Faraday constant ($C\cdot mol^{-1}$), molar gas constant ($J\cdot K^{-1}\cdot mol^{-1}$), and temperature (K), respectively.

2.2.2 SP from electrokinetic origin

The electrokinetic phenomenon occurs due to the charge separation at mineral−water interfaces, where an excess of (typically negative) charge remains on the mineral surface, and the excess (usually positive) countercharges stay in the water adjacent to the mineral surface. Such a model is known as the electric double layer [43,57,69,70]. As water flows through the pore space, some of the countercharges in the diffusion layer are transported by the flow, thus forming the streaming current and resulting in the streaming (or electrokinetic) potential.

2.2.3 SP from thermoelectric origin

Thermoelectric potentials occur when a change in temperature causes charge transport, during which the heat gradient creates a gradient in chemical potentials, resulting in ionic migration at different rates [56]. The presence of the electric double layer also contributes to the ionic migration due to temperature gradients.

2.3 Instrumentation and measurement

2.3.1 Instrumentation

The basic equipment required for SP data acquisition in most situations is simple, including (1) a pair or an array of non-polarized electrodes, (2) a high input-impedance measurement device (e.g., ~$10^8\,\Omega$), and (3) insulated connecting wires. The non-polarized electrode typically comprises a metal (such as Cu, Ag and Pb) immersed in a solution of a salt of the metal (e.g., $CuSO_4$, AgCl and $PbCl_2$) [3]. Ag−AgCl, Cu−$CuSO_4$ and

$Pb-PbCl_2$ electrodes are the most widely used non-polarized electrodes [6,18,27,29,34,51], where the $Cu-CuSO_4$ electrodes are more suitable for SP measurements in the field [71], and Ag−AgCl electrodes are more suitable for laboratory measurements [72]. It is noted that even using these non-polarized electrodes, polarization and drift may be significant sources of error in SP surveys [3].

2.3.2 Measurement

Laboratory measurement: The laboratory measurements often aim to determine the values of the coupling coefficient. There are three types of measurements: streaming potential measurements [70,73], measurements of electrochemical origins (e.g., exclusion-diffusion potentials [3] and redox potentials [12,13]), and thermoelectric potential measurements [74].

Borehole measurement: The borehole measurements are acquired using a logging tool, during which a downhole electrode connected to a reference electrode on the surface measures the electric potential through a high-resistance voltmeter and an adjustable voltage source. The use of the adjustable voltage source aims to allow the measured potential to be canceled out to generate a baseline signal of zero [75].

Ground measurement: Ground measurements have two commonly-used ways. The first one named the fixed-base method is combined with a fixed electrode at the base station as the common (or reference) electrode while the roving electrode moves at a regular interval to scan the electric potential on the ground surface. The fixed-base method can effectively reduce cumulative errors and electro-telluric noise caused by variations of the earth's magnetic field and industry sources [76]. Another one is the gradient method (also termed the dipole, leapfrog, or fixed electrode configuration), where two electrodes move simultaneously for each measurement, i.e., after finishing the measurement of the potential difference at a station, the two electrodes move along the survey line with the trailing electrode occupying the station of the previous leading electrode [3,76]. The gradient method is time-consuming, and noise potentials will accumulate.

Underwater measurement: Underwater measurements, mainly aiming at marine mineral or hydrothermal exploration, typically have two types. The conventional underwater measurement employs a deep-towed electrode array attached to a ship via a communication cable to measure the horizontal distribution of electric fields or potentials [14,17,18,20−22,24,29]. This way has some defects, such as inconvenient deep-sea operations, not suitable for complex submarine terrain, and low efficiency [77]. Another emerging and popular measurement is to use autonomous underwater vehicles (AUV) as carriers to conduct SP measurements. There are two types of devices. One is to arrange the towed electrode array on the tail of the AUV to record the horizontal electric fields or potentials [16,25,27,78]. The other is to attach non-polarized electrodes to the AUV to measure the horizontal and vertical electric fields or potentials [26,77,79]. AUV measurements have many advantages, such as being less susceptible to complex submarine environments, being able to take measurements at set speeds along set routes, and being efficient. Also, AUVs can be equipped with multiple geophysical instruments and can measure multiple geophysical data simultaneously [26,80]. Because of the high efficiency, economic benefit, and data richness, AUV measurements have been playing an important role in marine SP surveys.

3 Forward and inversion

3.1 Numerical modeling

In geophysics, numerical modeling is a qualitative (or semi-quantitative) technique, which employs the mathematical−physical equations governing the objective geophysical property, numerical modeling algorithms (or analytic solutions), and distributions of model parameters to simulate the geophysical response induced by causative sources. And then, responses are further analyzed to infer some additional information about the geophysical model. Numerical modeling also provides the forward process for inversion, aiming to achieve quantitative (or semi-quantitative) interpretation of observed geophysical data.

3.1.1 Poisson equation

For SP models, there are mainly two kinds of numerical models. One is described by the Poisson equation as given in Eq. (4), which should be solved using numerical modeling algorithms, e.g.,

commonly-used finite element method (FEM) [81], finite difference method (FDM) [10], and finite volume method (FVM) [82]. Recently, some coupled numerical algorithms have also shown good results. For example, XIE et al [66] proposed a coupled method by integrating the FEM and the infinite element method (IFEM) to perform the numerical modeling of SP signals from a simplified biogeobattery model in an organic-rich contaminated site. XIE et al [67] adopted the same coupled method to study the SP distribution pertaining to SMS deposits. XIE et al [83] also proposed a new interpolation function for multi-directional mapping IFEM and used the improved coupled method of the FEM and IFEM to describe seepage SP anomalies. Besides, XIE et al [84] proposed the natural-infinite element coupling method by integrating the natural element method (NEM) and the IFEM to conduct the forward modeling of SP signals generated by biogeobattery models. In the above examples, the finite elements and/or the natural elements (or natural nodes) play the role to discretize and fill the study area, while the infinite elements aim to act as boundary elements and deal with the truncated boundary problems. The distinct advantage of the coupled method is that it avoids artificial boundary conditions, which is a troublesome problem in multi-source models [67] or dynamic-source models [83].

In the forward modeling process, the Poisson equation can be written in a matrix form $\boldsymbol{Km}=\boldsymbol{d}$, where $\boldsymbol{K}$ is the Kernel matrix about conductivity distributions and derived from numerical modeling algorithms (e.g., the FEM, FDM, FVM, and the coupled method), $\boldsymbol{m}$ is the source vector, and $\boldsymbol{d}$ is the calculated SP data. In the coupled method, $\boldsymbol{K}$ is independent of $\boldsymbol{m}$, which helps to simplify the calculation process for both forward and inversion. $\boldsymbol{K}$ is generally computed by integrating the study area, which can be expressed as (take hexahedral elements as an example)

$$K_{ij}=\sigma\int_{-1}^{1}\int_{-1}^{1}\int_{-1}^{1}\left[\frac{\partial N_i}{\partial x}\frac{\partial N_j}{\partial x}+\frac{\partial N_i}{\partial y}\frac{\partial N_j}{\partial y}+\frac{\partial N_i}{\partial z}\frac{\partial N_j}{\partial z}\right]\cdot \boldsymbol{J}_{\mathrm{a}}\mathrm{d}\xi\mathrm{d}\eta\mathrm{d}\zeta \tag{6}$$

where K_{ij} represents the stiffness value, N means the interpolation function, ξ, η and ζ are local coordinates of the integral element, $i, j = 1, 2, \cdots, 8$, and $\boldsymbol{J}_{\mathrm{a}}$ is the Jacobi matrix and can be written as

$$\boldsymbol{J}_{\mathrm{a}}=\begin{bmatrix}\dfrac{\partial x}{\partial\xi} & \dfrac{\partial y}{\partial\xi} & \dfrac{\partial z}{\partial\xi}\\ \dfrac{\partial x}{\partial\eta} & \dfrac{\partial y}{\partial\eta} & \dfrac{\partial z}{\partial\eta}\\ \dfrac{\partial x}{\partial\zeta} & \dfrac{\partial y}{\partial\zeta} & \dfrac{\partial z}{\partial\zeta}\end{bmatrix}=\sum_{i=1}^{8}\begin{bmatrix}\dfrac{\partial M_i}{\partial\xi}x_i & \dfrac{\partial M_i}{\partial\xi}y_i & \dfrac{\partial M_i}{\partial\xi}z_i\\ \dfrac{\partial M_i}{\partial\eta}x_i & \dfrac{\partial M_i}{\partial\eta}y_i & \dfrac{\partial M_i}{\partial\eta}z_i\\ \dfrac{\partial M_i}{\partial\zeta}x_i & \dfrac{\partial M_i}{\partial\zeta}y_i & \dfrac{\partial M_i}{\partial\zeta}z_i\end{bmatrix}=\begin{bmatrix}\dfrac{\partial M_1}{\partial\xi} & \dfrac{\partial M_2}{\partial\xi} & \cdots & \dfrac{\partial M_8}{\partial\xi}\\ \dfrac{\partial M_1}{\partial\eta} & \dfrac{\partial M_2}{\partial\eta} & \cdots & \dfrac{\partial M_8}{\partial\eta}\\ \dfrac{\partial M_1}{\partial\zeta} & \dfrac{\partial M_2}{\partial\zeta} & \cdots & \dfrac{\partial M_8}{\partial\zeta}\end{bmatrix}\begin{bmatrix}x_1 & y_1 & z_1\\ x_2 & y_2 & z_2\\ \vdots & \vdots & \vdots\\ x_8 & y_8 & z_8\end{bmatrix} \tag{7}$$

where M represents the mapping function in the IFEM [66,67,83,84] and the interpolation function in the FEM [66,67,83] or NEM [84], respectively, and $x_1, x_2, \cdots, x_8, y_1, y_2, \cdots, y_8$, and $z_1, z_2, \cdots, z_8$ are real coordinates of the integral element.

The above calculation processes derived from the Poisson equation are suitable for different kinds of numerical modeling algorithms. In order to obtain the SP distribution ($\boldsymbol{d}$) in SP models, the conductivity (or resistivity) information should be available; however, the SP current density $\boldsymbol{J}_{\mathrm{SP}}$ ($\boldsymbol{m}$), contributed by different source mechanisms, is still hard to determine quantitatively. In mineral exploration, the SP signal in the triggering of ore bodies is always associated with redox potentials, which makes it possible to calculate SP sources. For example, STOLL et al [62] and BIGALKE and GRABNER [68] derived the inert electrode model (IEM) based on the classical electrochemical model proposed by BOCKRIS and REDDY [85] to quantitatively determine SP sources related to the orebody polarization. MENDONÇA [10] applied the IEM for forward and inversion in on-land mineral exploration. Recently, XIE et al [67] introduced this model to marine mineral exploration. All the above studies focus primarily on solving the

Poisson equation to obtain SP distributions, while for some simple models, the analytic solution works well on approximately interpreting SP signals.

3.1.2 Analytic solution for special geometry shape

Another numerical model, the analytic solution, different from solving the Poisson equation is to use some idealized geometry shapes to characterize the structure of underground ore bodies, thus the surface SP signals can be calculated analytically. In this model, SP anomalies depend on the locations of positive and negative poles, electric dipole density, and the shape of the causative bodies [86,87]. In most studies, mineralization is usually represented by some special geometry shapes such as spherical bodies, horizontal and vertical cylindrical bodies, and thin and thick sheet-type (vertical, dipping, or horizontal) structures [88] to simplify the forward modeling process. Point-by-point numerical modeling of different subsurface idealized geological bodies is summarized below.

Regular-shaped geometrical body: The SP anomaly $\varphi(x)$ along a profile passing over the center of a sphere or a vertical cylinder or along with a profile normal to the strike of a horizontal cylinder (e.g., Figs. 2(a) and (b)) can be expressed as [88−90]

$$\varphi(x)=k\frac{[(x-x_0)\cos\theta+h\sin\theta]}{[(x-x_0)^2+h^2]^q} \tag{8}$$

where k is the polarization parameter, x_0 is the x coordinate of the center of the causative body, h is the depth to the center for sphere and horizontal cylinder and depth to the top for vertical cylinder, θ is the polarization angle, and q is the shape factor [87]. The shape factors are 1.5, 1.0 and 0.5 for the sphere, horizontal cylinder and vertical cylinder, respectively [89].

2D inclined thin sheet-type body: An inclined thin sheet-type structure (see Fig. 2(c)) in 2D, which represents thin sheet interconnected graphite precipitation on fault planes [62], can be described by electric dipole density k, x coordinate of the center of the sheet x_0, depth of the center of the sheet h, half-width of the sheet a, and inclination angle α. The general expression of SP anomaly $\varphi(x)$ at any point on profile can be written as [88,91,92]

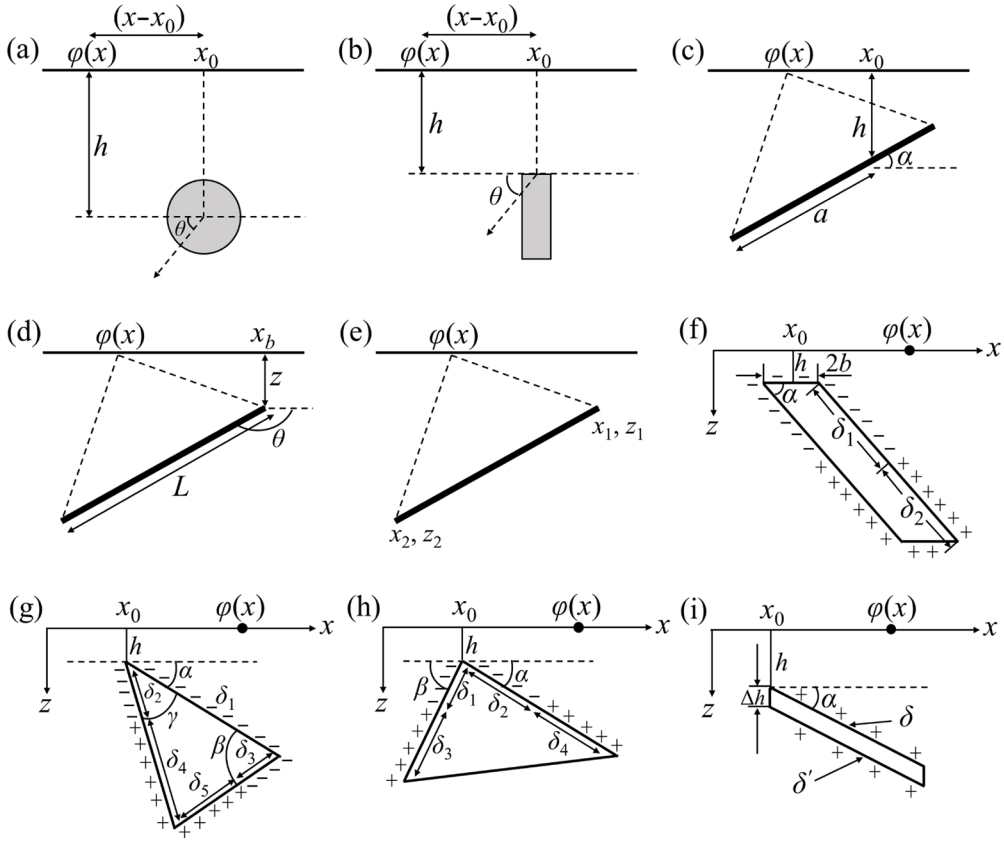

Fig. 2 Geometrical shaped body: (a) Sphere and horizontal cylinder; (b) Vertical cylinder; (c, d, e) 2D inclined thin sheet geometry of infinite horizontal extent; (f) Thick prismatic dipping layer; (g) Infinitely striking downward trihedral prism; (h) Infinitely striking upward trihedral prism; (i) Infinitely striking thin sheet layer (Redrawn from Ref. [88])

$$\varphi(x)=k\ln\left\{\frac{[(x-x_0)-a\cos\alpha]^2+(h-a\sin\alpha)^2}{[(x-x_0)+a\cos\alpha]^2+(h+a\sin\alpha)^2}\right\} \quad (9)$$

Besides, when sheet model parameters are described by one edge of the sheet (see Fig. 2(d)), the SP anomaly $\varphi(x)$ along a profile can be written as [88,93]

$$\varphi(x)=k\ln\left\{\frac{(x-x_{\mathrm{b}})^2+z^2}{[x-(x_b+L\cos\theta)]^2+(z+L\sin\theta)^2}\right\} \quad (10)$$

where x_{b} and z define the location of the upper edge of the sheet, L is the extent of the sheet, and θ is the angle of the sheet in a clockwise direction from the positive x-axis.

When model parameters are described by x and z coordinates of the upper and lower edges of the sheet, the SP anomaly $\varphi(x)$ of a sheet-like body (see Fig. 2(e)) can be written as [88,93]

$$\varphi(x)=k\ln\left[\frac{(x-x_1)^2+{z_1}^2}{(x-x_2)^2+{z_2}^2}\right] \quad (11)$$

where x_1, z_1, and x_2, z_2 are the coordinates of the top and bottom ends of the sheet, respectively.

Thick prismatic dipping body: The SP anomaly $\varphi(x)$ at any point on the surface of the profile due to a thick dipping body (see Fig. 2(f)) can be expressed as [94]:

$$\begin{aligned}\varphi(x)=\frac{\varphi_0}{\pi}\Bigg[\Bigg(&-2\arctan\frac{x_0-x-b+\delta_1\cos\alpha}{h+\delta_1\sin\alpha}+\\&\arctan\frac{x_0-x-b+(\delta_1+\delta_2)\cos\alpha}{h+(\delta_1+\delta_2)\sin\alpha}+\\&\arctan\frac{x_0-x-b}{h}\Bigg)+\\&\left(\arctan\frac{x_0-x+b}{h}-\arctan\frac{x_0-x-b}{h}\right)+\\&\Bigg(-2\arctan\frac{x-x_0-b-\delta_1\cos\alpha}{h+\delta_1\sin\alpha}+\\&\arctan\frac{x-x_0-b-(\delta_1+\delta_2)\cos\alpha}{h+(\delta_1+\delta_2)\sin\alpha}+\\&\arctan\frac{x-x_0-b}{h}\Bigg)\Bigg]\end{aligned} \quad (12)$$

Downward trihedral prism: The SP anomaly $\varphi(x)$ at any point on the surface of the profile due to a downward trihedral prism (see Fig. 2(g)) can be expressed as [94]

$$\begin{aligned}\varphi(x)=\frac{\varphi_0}{\pi}\Bigg[\Bigg(&\arctan\frac{x_0-x}{h}-\\&2\arctan\frac{x_0-x+\delta_2\cos(\alpha+\gamma)}{h+\delta_2\sin(\alpha+\gamma)}+\\&\arctan\frac{x_0-x+(\delta_2+\delta_4)\cos(\alpha+\gamma)}{h+(\delta_2+\delta_4)\sin(\alpha+\gamma)}\Bigg)+\\&\left(\arctan\frac{x_0-x+\delta_1\cos\alpha}{h+\delta_1\sin\alpha}-\arctan\frac{x_0-x}{h}\right)+\\&\Bigg(2\arctan\frac{x-x_0-\delta_1\cos\alpha+\delta_3\cos(\beta-\alpha)}{h+\delta_1\sin\alpha+\delta_3\sin(\beta-\alpha)}-\\&\arctan\frac{x-x_0-\delta_1\cos\alpha+(\delta_3+\delta_5)\cos(\beta-\alpha)}{h+\delta_1\sin\alpha+(\delta_3+\delta_5)\sin(\beta-\alpha)}-\\&\arctan\frac{x-x_0-\delta_1\cos\alpha}{h+\delta_1\sin\alpha}\Bigg)\Bigg]\end{aligned} \quad (13)$$

Upward trihedral prism: The SP anomaly $\varphi(x)$ at any point on the surface of the profile due to an upward trihedral prism (see Fig. 2(h)) can be expressed as [94]

$$\begin{aligned}\varphi(x)=\frac{\varphi_0}{\pi}\Bigg[\Bigg(&\arctan\frac{x_0-x}{h}-\\&2\arctan\frac{x_0-x-\delta_1\cos\beta}{h+\delta_1\sin\beta}+\\&\arctan\frac{x_0-x-(\delta_1+\delta_3)\cos\beta}{h+(\delta_1+\delta_3)\sin\beta}\Bigg)+\\&\Bigg(\arctan\frac{x-x_0}{h}-2\arctan\frac{x-x_0-\delta_2\cos\alpha}{h+\delta_2\sin\alpha}+\\&\arctan\frac{x-x_0-(\delta_2+\delta_4)\cos\alpha}{h+(\delta_2+\delta_4)\sin\alpha}\Bigg)\Bigg]\end{aligned} \quad (14)$$

Thin sheet-like dipping layer: The SP anomaly $\varphi(x)$ at any point on the surface of the profile due to a thin sheet-like dipping layer (see Fig. 2(i)) can be expressed as [94]

$$\begin{aligned}\varphi(x)=\frac{\varphi_0}{\pi}\Bigg[&\left(\arctan\frac{x_0-x+\delta\cos\alpha}{h+\delta\sin\alpha}-\arctan\frac{x_0-x}{h}\right)+\\&\left(\arctan\frac{x_0-x+\delta'\cos\alpha}{(h+\Delta h)\delta'\sin\alpha}-\arctan\frac{x_0-x}{h+\Delta h}\right)\Bigg]\end{aligned} \quad (15)$$

Dipping layer with variable dip (kink layer): Dipping layers with variable dip (kink layers) can also resemble an ore body embedded in the subsurface [94]. The SP anomaly $\varphi(x)$ at any point

on the surface of the profile due to a dipping layer with variable dip follows the principle of superposition [95] and can be added up through Eqs. (12) and (15) [94].

In Eqs. (12)−(15), φ_0 is the SP of the layer, h is the depth to the body top, b is the half-width (horizontal size) of the upper edge $2b$, x_0 corresponds to the center of the upper edge along the x-axis, x corresponds to the measuring point along the x-axis for which the potential is calculated, α, β and γ are the dip angles, δ, δ', δ_1, δ_2, δ_3, δ_4 and δ_5 are the lengths of sides or their negative and positive segments, respectively [94]. Based on the above-mentioned analytic solutions, we can conduct the forward modeling of most of the SP models in mineral exploration using one or a combination of them.

3.2 Inversion and interpretation

Forward modeling obtains the geophysical responses from the known model parameters through numerical algorithms or analytic solutions. In contrast, inversion aims to retrieve the unknown model parameters from a given set of observed data by repeating forward modeling processes. At each iteration step, the model parameters are improved to polish the initial model and better fit the observed data and calculated data. The iteration process continues until the stop criterion is reached. Data misfits or errors are represented by objective functions. Different inversion algorithms provide different ways to update the iteration process to minimize the objective function. Inverting SP data for interpretation is a typical potential field problem, of which the solution is known to be ill-posed and non-unique [96], i.e., an infinite number of source configurations can generate the same observed data. It is important to add additional constraints or prior information about the number of sources or the spatial extension of the source to reduce the space of the solution.

There are three scenarios for interpreting SP data. One involves the forward process based on the Poisson equation, for example, the forward process related to ore bodies is to solve the Eqs. (4) and (5) to obtain SP distributions. The second type, commonly used in mineral exploration, requires matching observed SP data with synthetic signals generated from simple geometrical models (as discussed in Section 3.1.2). The third one mainly includes some subjective interpretation methods. Details about the three types of SP inversion or interpretation are given below.

The first type requires prior information about the model (e.g., SP sources, and electric conductivity distributions), a forward modeling algorithm (e.g., FEM, FVM, FDM, and the coupled method), and an appropriate inversion algorithm (e.g., linear and non-linear). The purpose of inversion is to determine the best distribution of the source current density $\boldsymbol{m}$ by fitting the observation data $\boldsymbol{d}$ based on a known $\boldsymbol{K}$. Because $\boldsymbol{m}$ has a large number of parameters that determine the position and amplitude of SP sources, the most commonly used method for inversion in this type is linear inversion algorithms, e.g., least-squares algorithm (LSA) [10,12,13,36] and Gauss-Newton method (GNM) [40]. For example, MENDONÇA [10] used the LSA to invert the current source term based on SP data sets and a known resistivity model to explain SP anomalies in gold prospecting. CASTERMANT et al [12] and RITTGERS et al [13] employed the LSA to recover the source distribution from SP signals induced by lab-based redox processes. LINDE and REVIL [36] also conducted the LSA inversion to interpret the redox potential in contaminant plumes. For the GNM, MINSLEY et al [40] used it to estimate the source vector in combination with a conjugate gradient scheme to compute matrix inverses. JARDANI et al [44,97] also reported similar inversion cases directly based on the Tikhonov regularization solutions [96]. In other unusual cases, for example, MINSLEY et al [98] and LINDE et al [99] used model regularization with source compact to determine the source vector. LINDE et al [100] estimated the geometry of the ground water table by integrating SP and piezometric data using a Bayesian approach. ARORA et al [35] also adopted the same Bayesian method as LINDE et al [100] to remove the streaming potential component from in-situ SP data in contaminated sites.

In the second type, the results of curve modeling can determine the location and shape of SP sources (e.g., the polarization amplitude, the depth, the polarization angle, and the shape factor). The LSA and GNM have been widely used in these models [101−103]. Recently, there has been increasing interest in the application of global optimization (GO) techniques to geophysical

problems. This is because (1) there is no need to determine the Jacobian matrix, and (2) it can search for the whole model space and obtain the global optimum solution. Because model parameters are greatly reduced in the simplified SP models, the nonlinear GO algorithms are available to recover the idealized structures in mineral exploration. There have been many successful applications, including the black hole algorithm [104], the crow search algorithm [105], the differential evolution algorithm [106,107], the flower pollination algorithm [108], the fair function algorithm [109], the genetic algorithms [110], the genetic-price algorithm [111], the grey wolf optimizer [112], neural networks [113], the particle swarm optimization [114−116], the (very fast) simulated annealing algorithm [117,118], and the whale optimization algorithm [119].

The third group of inversion algorithms, such as characteristic points [120], nomograms [91], derivative analysis [101], spectral analysis [121,122], the depth from extreme points [123], and logarithmic-curve matching [124], also work for the SP signals generated by simple geometry structures; however, the drawback with these approaches is that they are highly subjective and hence may lead to major errors.

In general, linear inversion algorithms like the LSA and GNM are more suitable for recovering the current source vector in the inversion where the Poisson equation needs to be solved, while the GO technique seems to be better for the idealized ore-body structures.

4 Application in marine mineral exploration

4.1 Seafloor massive sulfide exploration

Mineral resources on land are increasingly exhausted; however, in marine environments, sulfide ore deposits, often accompanied by seafloor hydrothermal systems [125], have been regarded as submarine mineral resources to be explored and mined [126]. Hydrothermal deposits are large-scale geochemical anomalies of sulfur, and metallic sulfide minerals in hydrothermal deposits are the main economic minerals in the crust. SMS mineralization typically occurs at marine plate boundaries, such as mid-ocean ridges, volcanic arcs, and back-arc basins, where hydrothermal fluids erupt from deep in the crust, mix with cold seawater, and precipitate minerals on or below the sea-floor [127]. SMS is the primary source of the base metals Cu, Zn and Pb and a large number of lower-concentration metals including Ag, As, Au, Bi, Cd, Co, Ga, Ge, In, Hg, Mo, Ni, Re, Sb, Se, Sn, Te and Tl, and these metals typically form their sulfides or appear as trace elements in other sulfides and sulfosalts [128].

Geophysical techniques can provide efficient non-intrusive methods for detecting hidden minerals in terrestrial and marine environments. Active source methods like induced polarization (IP) [129,130], electrical resistivity tomography (ERT) [11,131], the time domain (transient) electromagnetic method (TEM) [132,133], and the controlled source frequency domain electromagnetic method (CSEM) [134,135] have been applied in on-land and/or marine mineral exploration. TEM and CSEM are more popular because the sensors can be towed by a ship for continuous measurements in marine environments. Some surveys combine two (e.g., SP and ERT [136]) or more (e.g., SP, ERT, and IP [11]) of them for prospecting. Passive methods like gravity surveys [137] and the geomagnetic method [138,139] are alternative techniques for exploring SMS; however, the magnetic method responds to any magnetized/ less-magnetized body, thus this method requires geological information about the target area. The plume survey method is also used in marine mineral exploration [140]. This method only responds to signals of plume fluids, while the fluid discharge location is sometimes different from the plume fluid location, thus may lead to the wrong delineation [25]. Compared with the above techniques, the SP method has a direct response to ore bodies due to redox reactions as described by the geobattery model, thus being more suitable for SMS prospecting.

The earliest and the most popular application of the SP method has been in mineral exploration since 1830 when Fox first observed negative SP anomalies related to sulfide deposits [2]. In the early state, the SP method is mainly applied to on-land mineral exploration [6−11]. Over the last nearly half a century, the SP method has been increasing interest in detecting SMS deposits after CORWIN's work [14]. Compared with on-land mineral exploration, marine SP signals generated by

seabed mineralization can be detected using relatively simple instruments towed behind ships or AUVs. SP measurements in seawater have some advantages that the noise level is significantly reduced, the contact resistance of seawater to the electrode is low (usually <1 Ω), the temperature and salinity of seawater are stable over time, meteorological and hydrogeological factors are reduced, and marine SP surveys are efficient and enable continuous measurements [14,17]. There have been lots of marine SP surveys aiming to detect the SMS deposits. For example, BREWITT-TAYLOR [78] performed deep-sea trials of SP measurements at Mid-Atlantic Ridge (MAR) to detect SMS deposits. CORWIN began to develop the marine SP observation system in 1973 [141] and observed an SP anomaly related to offshore extensions of the onshore deposits in 1976 [14]. von HERZEN et al [16] used an electrode array towed behind the submersible device Alvin and recorded negative potentials above the TAG hydrothermal mound. HEINSON et al [17] conducted two marine SP measurements in the south of Eyre Peninsula, South Australia, Rose Canyon, San Diego, and California. HEINSON et al [18] performed an SP measurement on the continental shelf of South Australia and suggested that the SP signals are probably due to the reduction−oxidation process across the conductive orebody below the seafloor because SP and magnetic data show limited spatial relevance. BELTENEV et al [20−22] conducted integrated geological−geophysical surveys to detect hydrothermal activity and sulfide mineralization within the MAR rift valley. CHERKASHOV et al [142,143] found a sulfide mineralization area in the inactive hydrothermal field at MAR. Recently, SAFIPOUR et al [23] made marine SP measurements over a known SMS deposit at the Palinuro Seamount in the Tyrrhenian Sea and observed SP signals at the site of SMS mineralization. KAWADA and KASAYA [24] observed negative SP anomalies over the SMS deposits in the Izena geothermal field. WANG et al [144] studied SP observation ways in detecting SMS deposits and provided a suggestion that gradient measurements are more suitable for offshore exploration. KASAYA et al [27,28] developed a system to monitor the sub-seafloor resistivity and SP concerning the physicochemical properties of ore deposits and the existence of hydrothermal fluid.

For data acquisition in the marine environment, in the early days, most SP studies typically used cables terminated with electrodes as the sensor and towed inline behind a ship [14,17,18,20−22,24,29]. Towed arrays have many limitations as discussed in Section 2.3. Therefore, AUVs equipped with SP instruments are introduced for marine SP measurements. For example, KAWADA and KASAYA [25] performed an SP survey using an AUV above the Sunrise deposit in the Myojin Knoll caldera of the Izu-Ogasawara arc. CONSTABLE et al [26] conducted three-component electric field observations using a commercial AUV. KASAYA et al [27] used multiple AUVs without a towing electrode cable for marine direct current resistivity and SP surveys. ZHU et al [77] built a new multicomponent electrical field observation system attached to an AUV. Due to the above successful cases of SP methods in marine mineral exploration, three field cases are given below to show the latest progress and application effect of SP surveys in marine prospecting.

4.2 Field Case I

The field Case I is from KAWADA and KASAYA [25]. The study area, Myojin Knoll, is located in the Izu-Ogasawara arc, southern Japan. The known Sunrise deposit has a size of about 400 m × 400 m [32]. The survey was composed of two groups of survey lines (a total of 12 lines) using the AUV Jinbei [145]. The origin point was chosen near the center of the deposit. Integrating the electric field along the survey lines can produce a negative SP anomaly (about 300 m × 300 m) with an amplitude of a few millivolts, and there is no strong SP anomaly outside of the Sunrise deposit.

The SP anomaly in the present survey agrees well with the results of an earlier survey by IIZASA et al [32]. KAWADA and KASAYA [25] applied the probability tomography method proposed by REVIL et al [146] and point source inversion to image a southward-dipping dipole with a moment of approximately 1.4×10^3 A·m and about 30 m below the southern part of the ore deposit, which indicates that the SP signals are probably contributed by the geobattery mechanism. The contribution of hydrothermal fluids to the SP anomalies is probably a secondary effect.

4.3 Field Case II

The field Case II is from CONSTABLE et al [26]. The study area is close to the Iheya Minor Ridge in the Iheya prospect of the Okinawa Trough, where there are active hydrothermal circulation and known SMS deposits [147]. A three-axis electric field receiver (Ag−AgCl electrodes) was mounted to the hard lifting points of the AUV to record the crossline, inline, and vertical electric fields. The SP distribution was reconstructed from the horizontal electric field data, where the largest anomaly is slightly over 25 mV and is located north of the center of the survey area, and a smaller 15 mV anomaly is located south over the area of the highest bathymetric relief, and the low SP extends along with the ridge structure to the northeast of the survey area.

Marine SP anomalies are generally contributed by either hydrothermal circulation (electrokinetic and/or thermoelectric phenomena) or the geobattery effect (electrochemical mechanisms). For the former, for example, YAMAMOTO et al [148] measured negative potentials related to hydrothermal fluids. For the latter, CORWIN [14] noted that measurements in marine sediments show lower oxidation potentials, which proves the assumption that SP anomalies generated by the geobattery mechanism are expected to be dipolar in nature. von SAFIPOUR et al [23] and KAWADA and KASAYA [24] observed near-seafloor dipolar anomalies and interpreted them as caused by the geobattery mechanism [4] over SMS deposits. In this case, although high conductivity suggests that the anomaly is associated with seafloor mineralization, CONSTABLE et al [26] thought that the source mechanism is more likely due to hydrothermal vents. If the source of the SP anomalies is SMS mineralization, there should be less localized and more dipolar SP signals.

4.4 Field Case III

The field Case III is from ZHU et al [29]. The study area is located at the Yuhuang seamount on the ultraslow-spreading Southwest Indian Ridge (SWIR). Two sulfide deposits with a diameter of about 500 m have been reported on the northwestern slope of the Yuhuang seamount [149]. The hydrothermal field is likely inactive, which is good for testing the ability of the SP survey to characterize buried SMS deposits. In this case, the obvious negative SP anomaly is more than 20 mV in the middle of the two survey lines, which is located in the region of the known mineralization area. The SP anomalies measured at the Yuhuang seamount are more likely related to inactive SMS deposits instead of electrokinetic contributions of an active vent because there are no water plume (temperature/turbidity) anomalies associated with active vents and SP signals pertaining to ore deposits are generally much stronger than electrokinetic contributions [25,150]. Besides, laboratory observations of SMS samples suggest that the outcrop sulfides primarily contain pyrite, chalcopyrite, and sphalerite, with ferric hydroxides identified on the surface of the samples. Similar pyrite samples also show high conductivity [134], which means that the conductive minerals are physically connected rather than other electron transfer mechanisms [134,151]. This study further strengthens the geobattery theory.

5 Discussion

In marine SP surveys, detailed geological information is not necessary when detecting ore deposits. However, geological information may provide additional constraints to support the investigation and facilitate inversion and interpretation. Bathymetry, for example, is important, which highlights the importance of the AUV because it can measure SP data at the same time as bathymetry. For greater efficiency, the battery life and capacity of the AUV can be improved to ensure that a single dive can last longer allowing for a wider survey area, which is particularly necessary for mineral exploration. Meanwhile, AUVs should be more intelligent to adapt to the complex marine environment, thus reducing the workload of operators and avoiding human errors. Due to the fact that the instrument used for SP measurements is the same as a receiver unit of the electric/electromagnetic method, AUVs can measure a variety of geophysical data simultaneously, such as active electric and electromagnetic measurements, so that combined surveys of the target area are available to provide the electrical conductivity structure for the inversion and interpretation of SP data. The development of joint inversion for complementary geophysical data can better constrain the

non-uniqueness and improve the quantitative interpretation of SP data.

In addition, the mature (older) inactive hydrothermal fields tend to have larger ore bodies in density and size than younger ones; however, they are difficult or impossible to detect by other geophysical methods because they do not have water column anomalies, i.e., high-temperature plumes and turbidity resulting from active hydrothermal vents. The SP method is not easy to judge the contribution of ore bodies to SP anomaly when there are hydrothermal contributions. Therefore, we have a conclusion that for the SP method, the simplest, most effective, and most economical marine mineral exploration is to investigate mature inactive deposits.

6 Conclusions

(1) The SP method comprises the passive measurement of naturally occurring potential differences at the ground surface and in boreholes or (sea-)water. SP surveys have a number of advantages over other geophysical approaches, such as it is often cheaper and quicker to implement and field data can be obtained over large regions with dense sampling in both space and time. Most importantly, SP anomalies are directly related to the subsurface process of interest, such as changes in groundwater flow, chemistry, and temperature. The causative sources for SP signals arise (a) from a thermoelectric potential, a consequence of a temperature gradient, (b) from an electrochemical potential, a consequence of chemical gradients, and (c) from a streaming potential, electrokinetic phenomena, a consequence of fluid pressure gradients. The diversity of sources is both a strength and a weakness. Many phenomena can be studied with SP measurements; however, several different sources can sometimes be confusing.

(2) We use the SP method to address problems focusing mainly on mineral exploration due to the geobattery theory, environmental surveys commonly related to the biogeobattery theory and/or water flow, and hydrogeophysical issues typically associated with water flow. For mineral exploration, the geobattery model contributed from electrochemical mechanisms is suitable for both on-land and marine environments. The redox process forms a natural electric field, which can be observed by SP measurements. SP surveys require no detailed geological information for interpretation, which indicates that SP signals are linked directly to physicochemical processes inherent to ore deposits. Besides, mineral resources on land are increasingly depleted and difficult to explore and exploit. The marine mineral species are rich, and the geological conditions are simple. Marine SP surveys are more efficient due to the use of AUVs. Marine mineral exploration using SP surveys has become a new frontier and will certainly become an important research hotspot in the future.

(3) For environmental investigations, the corresponding SP contribution mainly comes from electrochemical and electrokinetic mechanisms, of which the former is from the redox reactions where bacteria participate. This bioelectrochemical system can be considered a biogeobattery model. The use of this SP anomaly is to monitor and delineate organic-rich contaminant plumes and DNAPL (or LNAPL). The electrokinetic component is due to the dissolution and diffusion of pollutants accompanying groundwater flow. In hydro-geophysical applications, SP contributions typically generated by electrokinetic phenomena have a linear relationship with subsurface water flow. This SP signal aims to detect, monitor, and delineate hydrogeophysical sites associated with groundwater flow. In order to conduct quantitative SP studies, other geophysical methods, such as ERT, IP, and GPR, must be included to assist in obtaining other useful geophysical properties, such as resistivity distributions.

(4) In summary, as one of the passive geophysical techniques, the SP method has the advantages of being non-invasive, simple equipment, low cost, and high efficiency, and has a unique response to underground causative sources. It is suitable for large-scale preliminary prospecting work qualitatively or semi-quantitatively, especially in mineral exploration, environmental surveys, and hydrogeophysical investigations. The interpretation would be better if combined with other geophysical methods.

Acknowledgments

This study is funded by the National Natural Science Foundation of China (Nos. 42174170, 41874145, 72088101).

References

[1] REVIL A, JARDANI A. The self-potential method: Theory and applications in environmental geosciences [M]. Cambridge: Cambridge University Press, 2013.

[2] FOX R W. On the electromagnetic properties of metalliferous veins in the mines of Cornwall [J]. Philosophical Transactions of the Royal Society of London, 1830, 120: 399−414.

[3] JACKSON M D. Tools and techniques: Self-potential methods [M]. 2nd ed. Oxford, UK: Elsevier, 2015: 261−293.

[4] SATO M, MOONEY H M. The electrochemical mechanism of sulfide self-potentials [J]. Geophysics, 1960, 25(1): 226−249.

[5] REVIL A, MENDONÇA C A, ATEKWANA E A, KULESSA B, HUBBARD S S, BOHLEN K J. Understanding biogeobatteries: Where geophysics meets microbiology [J]. Journal of Geophysical Research, 2010, 115: G00G02.

[6] EPPELBAUM L V. Advanced analysis of self-potential data in ore deposits of the South Caucasus [J]. ANAS Transactions, Earth Sciences, 2019, 2: 21−35.

[7] LOGN O, BØLVIKEN B. Self-potentials at the Joma pyrite deposit, Norway [J]. Geoexploration, 1974, 12: 11−28.

[8] CORRY C E. Spontaneous polarization associated with porphyry sulfide mineralization [J]. Geophysics, 1985, 50: 1020−1034.

[9] BHATTACHARYA B B, SHALIVAHAN J A, BERA A. Three-dimensional probability tomography of self-potential anomalies of graphite and sulphide mineralization in Orissa and Rajasthan, India [J]. Near Surface Geophysics, 2007, 5: 223−230.

[10] MENDONÇA C A. Forward and inverse self-potential modeling in mineral exploration [J]. Geophysics, 2008, 73(1): F33−F43.

[11] HORO D, PAL S K, SINGH S, SRIVASTAVA S. Combined self-potential, electrical resistivity tomography and induced polarization for mapping of gold prospective zones over a part of Babaikundi-Birgaon Axis, North Singhbhum Mobile Belt, India [J]. Exploration Geophysics, 2020, 51(5): 507−522.

[12] CASTERMANT J, MENDONÇA C A, REVIL A, TROLARD F, BOURRIÉ G, LINDE N. Redox potential distribution inferred from self-potential measurements associated with the corrosion of a burden metallic body [J]. Geophysical Prospecting, 2008, 56: 269−282.

[13] RITTGERS J B, REVIL A, KARAOULIS M, MOONEY M A, SLATER L D, ATEKWANA E A. Self-potential signals generated by the corrosion of buried metallic objects with application to contaminant plumes [J]. Geophysics, 2013, 78(5): EN65−EN82.

[14] CORWIN R F. Offshore use of the self-potential method [J]. Geophysical Prospecting, 1976, 24(1): 79−90.

[15] FRANCIS T J G. Resistivity measurements of an ocean floor sulphide mineral deposit from the submersible Cyana [J]. Marine Geophysical Researches, 1985, 7: 419−437.

[16] von HERZEN R P, KIRKLIN J, BECKER K. Geoelectrical measurements at the TAG hydrothermal mound [J]. Geophys Res Lett, 1996, 23: 3451−3454.

[17] HEINSON G, WHITE A, CONSTABLE S, KEY K. Marine self potential exploration [J]. Exploration Geophysics, 1999, 30: 1−4.

[18] HEINSON G, WHITE A, ROBINSON D, FATHIANPOUR N. Marine self-potential gradient exploration of the continental margin [J]. Geophysics, 2005, 70(5): G109−G118.

[19] SUDARIKOV S M, ROUMIANTSEV A B. Structure of hydrothermal plumes at the Logatchev vent field, 14°45′N, Mid-Atlantic Ridge: Evidence from geochemical and geophysical data [J]. Journal of Volcanology and Geothermal Research, 2000, 101: 245−252.

[20] BELTENEV V, IVANOV V, ROZHDESTVENSKAYA I, CHERKASHOV G, STEPANOVA T, SHILOV V, PERTSEV A, DAVYDOV M, EGOROV I, MELEKESTSEVA I, NARKEVSKY E, IGNATOV V. A new hydrothermal field at 13°30′N on the Mid-Atlantic Ridge [J]. Inter Ridge News, 2007, 16: 9−10.

[21] BELTENEV V, IVANOV V, ROZHDESTVENSKAYA I, CHERKASHOV G, STEPANOVA T, SHILOV V, PERTSEV A. New data about hydrothermal fields on the Mid-Atlantic Ridge between 11−14°N: 32nd Cruise of R/V Professor Logatchev [J]. Geochemistry Geophysics Geosystems, 2008, 10: 1029.

[22] BELTENEV V, IVANOV V, ROZHDESTVENSKAYA I, CHERKASHOV G, STEPANOVA T, SHILOV V, DAVYDOV M, LAIBA A, KAYLIO V, NARKEVSKY E, PERTSEV A, DOBRETZOVA I, GUSTAYTIS A, POPOVA Y E, AMPLIEVA Y E, EVRARD C, MOSKALEV L, GEBRUK A. New data about hydrothermal fields on the Mid-Atlantic Ridge between 11°−14°N: 32nd cruise of R/V Professor Logatchev [J]. InterRidge News, 2009, 18: 13−17.

[23] SAFIPOUR R, HÖLZ S, HALBACH J, JEGEN M, PETERSEN S, SWIDINSKY A. A self-potential investigation of submarine massive sulfides: Palinuro Seamount, Tyrrhenian Sea [J]. Geophysics, 2017, 82(6): A51−A56.

[24] KAWADA Y, KASAYA T. Marine self-potential survey for exploring seafloor hydrothermal ore deposits [J]. Scientific Reports, 2017, 7: 1−12.

[25] KAWADA Y, KASAYA T. Self-potential mapping using an autonomous underwater vehicle for the Sunrise deposit, Izu-Ogasawara arc, southern Japan [J]. Earth, Planets and Space, 2018, 70: 1−15.

[26] CONSTABLE S, KOWALCZYK P, BLOOMER S. Measuring marine self-potential using an autonomous underwater vehicle [J]. Geophysical Journal International, 2018, 215: 49−60.

[27] KASAYA T, IWAMOTO H, KAWADA Y, HYAKUDOME T. Marine DC resistivity and self-potential survey in the hydrothermal deposit areas using multiple AUVs and ASV [J]. Terr Atmos Ocean Sci, 2020, 31(5): 579−588.

[28] KASAYA T, IWAMOTO H, KAWADA Y. Deep-sea DC resistivity and self-potential monitoring system for environmental evaluation with hydrothermal deposit mining [J]. Frontiers in Earth Science, 2021, 9: 608381.

[29] ZHU Z, TAO C, SHEN J, REVIL A, DENG X, LIAO S, ZHOU J, WANG W, NIE Z, YU J. Self-potential tomography

of a deep-sea polymetallic sulfide deposit on Southwest Indian Ridge [J]. Journal of Geophysical Research: Solid Earth, 2020, 125: e2020JB019738.

[30] MINNITI M, BONAVIA F F. Copper-ore grade mineralization discovered in a seamount in the Tyrrhenian Sea (Mediterranean): Is the mineralization related to porphyry-coppers or to base metal lodes? [J]. Marine Geology, 1984, 59: 271−282.

[31] PETERSEN S, MONECKE T, WESTHUES A, HANNINGTON M D, GEMMELL J B, SHARPE R, PETERS M, STRAUSS H, LACKSCHEWITZ K, AUGUSTIN N, GIBSON H, KLEEBERG R. Drilling shallow-water massive sulfides at the Palinuro volcanic complex, Aeolian Island Arc, Italy [J]. Economic Geology, 2014, 109: 2129−2158.

[32] IIZASA K, FISKE R S, ISHIZUKA O, YUASA M, HASHIMOTO J, ISHIBASHI J, NAKA J, HORII Y, FUJIWARA Y, IMAI A, KOYAMA S. A kuroko-type polymetallic sulfide deposit in a submarine silicic caldera [J]. Science, 1999, 283: 975−977.

[33] YOSHIZUMI R, MIYOSHI Y, ISHIBASHI J I. The characteristics of the seafloor massive sulfide deposits at the Hakurei site in the Izena hole, the Middle Okinawa Trough [M]//Subseafloor Biosphere Linked to Hydrothermal Systems. Tokyo: Springer, 2015: 561−565.

[34] NAUDET V, REVIL A, RIZZO E, BOTTERO J Y, BÉGASSAT P. Groundwater redox conditions and conductivity in a contaminant plume from geoelectrical investigations [J]. Hydrology and Earth System Sciences, 2004, 8(1): 8−22.

[35] ARORA T, LINDE N, REVIL A, CASTERMANT J. Non-intrusive characterization of the redox potential of landfill leachate plumes from self-potential data [J]. Journal of Contaminant Hydrology, 2007, 92: 274−292.

[36] LINDE N, REVIL A. Inverting self-potential data for redox potentials of contaminant plumes [J]. Geophysical Research Letters, 2007, 34: L14302.

[37] MAO D, REVIL A, HORT R D, MUNAKATA-MARR J, ATEKWANA E A, KULESSA B. Resistivity and self-potential tomography applied to groundwater remediation and contaminant plumes: Sandbox and field experiments [J]. Journal of Hydrology, 2015, 530: 1−14.

[38] ABBAS M, JARDANI A, SOUEID AHMED A, REVIL A, BRIGAUD L, BÉGASSAT P, DUPONT J P. Redox potential distribution of an organic-rich contaminated site obtained by the inversion of self-potential data [J]. Journal of Hydrology, 2017, 554: 111−127.

[39] CUI Yi-an, ZHU Xiao-xiong, WEI Wen-sheng, LIU Jian-xin, TONG Tie-gang. Dynamic imaging of metallic contamination plume based on self-potential data [J]. Transactions of Nonferrous Metals Society of China, 2017, 27(8): 1822−1830.

[40] MINSLEY B J, SOGADE J, MORGAN F D. Three-dimensional self-potential inversion for subsurface DNAPL contaminant detection at the Savannah River Site, South Carolina [J]. Water Resources Research, 2007, 43: W04429.

[41] ATEKWANA E A, ATEKWANA E A. Geophysical signatures of microbial activity at hydrocarbon contaminated sites: A review [J]. Surv Geophys, 2010, 31: 247−283.

[42] KANG X, KOKKINAKI A, KITANIDIS P K, SHI X, REVIL A, LEE J, SOUEID AHMED A, WU J. Improved characterization of DNAPL source zones via sequential hydrogeophysical inversion of hydraulic-head, self-potential and partitioning tracer data [J]. Water Resources Research, 2020, 56: e2020WR027627.

[43] SILL W R. Self-potential modeling from primary flows [J]. Geophysics, 1983, 48(1): 76−86.

[44] JARDANI A, REVIL A, BOLÈVE A, CRESPY A, DUPONT J P, BARRASH W, MALAMA B. Tomography of the Darcy velocity from self-potential measurements [J]. Geophysical Research Letters, 2007, 34: L24403.

[45] CORWIN R F, MORRISON H F. Self-potential variations preceding earthquakes in central California [J]. Geophysical Research Letters, 1977, 4(4): 171−174.

[46] SOUEID AHMED A, REVIL A, BOLÈVE A, STECK B, VERGNIAULT C, COURIVAUD J R, JOUGNOT D, ABBAS M. Determination of the permeability of seepage flow paths in dams from self-potential measurements [J]. Engineering Geology, 2020, 268: 105514.

[47] BOLÈKVE J, REVIL A, JANOD F, MATTIUZZO J L, FRY J J. Preferential fluid flow pathways in embankment dams imaged by self-potential tomography [J]. Near Surface Geophysics, 2009, 7(5): 447−462.

[48] RIZZO E, SUSKI B, REVIL A, STRAFACE S, TROISI S. Self-potential signals associated with pumping tests experiments [J]. Journal of Geophysical Research, 2004, 109: B10203.

[49] REVIL A, NAUDET V, MEUNIER J D. The hydroelectric problem of porous rocks: Inversion of the position of the water table from self-potential data [J]. Geophysical Journal International, 2004, 159: 435−444.

[50] TITOV K V, LEVITSKI A, KONOSAVSKI P K, TARASOV A V, ILYIN Y T, BUÈS M A. Combined application of surface geoelectrical methods for groundwater-flow modeling: A case history [J]. Geophysics, 2005, 70(5): H21−H31.

[51] SUSKI B, REVIL A, TITOV K, KONOSAVSKY P, VOLTZ M, DAGÈS C, HUTTEL O. Monitoring of an infiltration experiment using the self-potential method [J]. Water Resources Research, 2006, 42: W08418.

[52] GRAHAM M T, MACALLISTER D J, VINOGRADOV J, JACKSON M D, BUTLER A P. Self-potential as a predictor of seawater intrusion in coastal groundwater boreholes [J]. Water Resources Research, 2018, 54: 6055−6071.

[53] FINIZOLA A, LÉNAT J F, MACEDO O, RAMOS D, THOURET J C, SORTINO F. Fluid circulation and structural discontinuities inside Misti volcano (Peru) inferred from self potential measurements [J]. Journal of Volcanology and Geothermal Research, 2004, 135(4): 343−360.

[54] AIZAWA K, OGAWA Y, ISHIDO T. Groundwater flow and hydrothermal systems within volcanic edifices: Delineation by electric self-potential and magnetotellurics [J]. Journal of Geophysical Research, 2009, 114: B01208.

[55] REVIL A, KARAOULIS M, SRIVASTAVA S, BYRDINA S. Thermoelectric self-potential and resistivity data localize the burning front of underground coal fires [J]. Geophysics, 2013, 78(5): B259−B273.

[56] REVIL A. Ionic diffusivity, electrical conductivity,

membrane and thermoelectric potentials in colloids and granular porous media: A unified model [J]. Journal of Colloid and Interface Science, 1999, 212: 503−522.

[57] REVIL A, PEZARD P A, GLOVER P W J. Streaming potential in porous media 1. Theory of the zeta potential [J]. Journal of Geophysical Research, 1999, 104(B9): 20021−20031.

[58] ONSAGER L. Reciprocal relations in irreversible processes I [J]. Phys Rev, 1931, 37: 405−426.

[59] NOURBEHECHT B. Irreversible thermodynamic effects in inhomogeneous media and their applications in certain geoelectric problems [D]. Cambridge, USA: Massachusetts Institute of Technology, 1963.

[60] MINSLEY B J. Modeling and inversion of self-potential data [D]. West Lafayette, USA: Purdue University, 1997.

[61] TELFORD W M, GELDART L P, SHERIFF R E. Applied geophysics [M]. 2nd ed. Cambridge: Cambridge University Press, 1990.

[62] STOLL J, BIGALKE J, GRABNER E W. Electrochemical modeling of self-potential anomalies [J]. Surveys in Geophysics, 1995, 16: 107−120.

[63] GORBY Y A, YANINA S, MCLEAN J S, ROSSO K M, MOYLES D, DOHNALKOVA A. Electrically conductive bacterial nanowires produced by *Shewanella oneidensis* strain MR-1 and other microorganisms [J]. Proceedings of the National Academy of Sciences of the United States of America, 2006, 103: 11358−11363.

[64] KATO S, HASHIMOTO K, WATANABE K. Microbial interspecies electron transfer via electric currents through conductive minerals [J]. Proceedings of the National Academy of Sciences of the United States of America, 2012, 109: 10042−10046.

[65] NTARLAGIANNIS D, ATEKWANA E A, HILL E A, GORBY Y. Microbial nanowires: Is the subsurface 'hardwired'? [J]. Geophysical Research Letters, 2007, 34: L17305.

[66] XIE J, CUI Y A, ZHANG L J, GUO Y J, WANG J X, FANIDI M, LIU J X. Numerical modeling of biogeobattery system from microbial degradation of underground organic contaminant [J]. SN Applied Sciences, 2020, 2: 208.

[67] XIE J, CUI Y A, FANIDI M, ZHANG L J, GUO Y J, LUO Y J, LIU J X. Numerical modeling of marine self-potential from a seafloor hydrothermal ore deposit [J]. Pure and Applied Geophysics, 2021, 178: 1731−1744.

[68] BIGALKE J, GRABNER E W. The geobattery model: A contribution to large-scale electrochemistry [J]. Electrochimica Acta, 1997, 42: 3443−3452.

[69] OVERBEEK J T. Colloid science [M]. New York: Elsevier, 1960.

[70] ISHIDO T, MIZUTANI H. Experimental and theoretical basis of electrokinetic phenomena in rock−water systems and its applications to geophysics [J]. Journal of Geophysical Research, 1981, 86(B3): 1763−1775.

[71] MAINALI G, NORDLUND E, KNUTSSON S, THUNEHED H. Tailings Dams monitoring in Swedish mines using self-potential and electrical resistivity methods [J]. Electronic Journal of Geotechnical Engineering, 2015, 20(13): 5859−5875.

[72] HUBBARD C G, WEST L J, MORRIS K, KULESSA B, BROOKSHAW D, LLOYD J R, SHAW S. In search of experimental evidence for the biogeobattery [J]. Journal of Geophysical Research, 2011, 116: G04018.

[73] AHMAD M U. A laboratory study of streaming potentials [J]. Geophysical Prospecting, 1964, 12(1): 49−64.

[74] LEINOV E, JACKSON M D. Experimental measurements of the SP response to concentration and temperature gradients in sandstones with application to subsurface geophysical monitoring [J]. Journal of Geophysical Research: Solid Earth, 2014, 119: 6855−6876.

[75] HEARST J R, NELSON P H, PAILLET F L. Well logging for physical properties [M]. Chichester: Wiley, 2000.

[76] CORWIN R F. The self-potential method for environmental and engineering applications [M]//Geotechnical and Environmental Geophysics. Society of Exploration Geophysicists, 1990: 127−146.

[77] ZHU Z M, SHEN J S, TAO C H, DENG X M, WU T, NIE Z F, WANG W Y, SU Z Y. Autonomous-underwater-vehicle-based marine multicomponent self-potential method: Observation scheme and navigational correction [J]. Geoscientific Instrumentation Methods and Data Systems, 2021, 10: 35−43.

[78] BREWITT-TAYLOR C R. Self-potential prospecting in the deep oceans [J]. Geology, 1975, 3(9): 541−542.

[79] CLAUS B, WEITEMEYER K, KOWALCZYK P, PROCTOR A, DONALD C, KOWALCZYK M. Autonomous underwater vehicle based electric and magnetic field measurements with applications to geophysical surveying and subsea structure inspection [C]//2020 IEEE/OES Autonomous Underwater Vehicles Symposium (AUV). Canada: IEEE, 2020: 1−5.

[80] CONSTABLE S, KANNBERG P K, WEITEMEYER K. Vulcan: A deeptowed CSEM receiver [J]. Geochem Geophys Geosyst, 2016, 17: 1042−1064.

[81] SOUEID AHMED A, JARDANI A, REVIL A, DUPONT J P. SP2DINV: A 2D forward and inverse code for streaming potential problems [J]. Computers & Geosciences, 2013, 59: 9−16.

[82] SHEFFER M R, OLDENBURG D W. Three-dimensional modelling of streaming potential [J]. Geophys J Int, 2007, 169: 839−848.

[83] XIE J, CUI Y A, ZHANG L J, MA C Y, YANG B, CHEN X L, LIU J X. 3D forward modeling of seepage self-potential using finite-infinite element coupling method [J]. Journal of Environmental and Engineering Geophysics, 2020, 25(3): 381−390.

[84] XIE J, CUI Y A, GUO Y J, ZHANG L J, FANIDI M, LIU J X. 2.5D self-potential forward modeling by natural-infinite element coupling method [J]. Journal of Applied Geophysics, 2020, 179: 104077.

[85] BOCKRIS J O' M, REDDY A K N. Modern electrochemistry [M]. New York: Plenum Press, 1970.

[86] ROUDSARI M S, BEITOLLAHI A. Forward modelling and inversion of self-potential anomalies caused by 2D inclined sheets [J]. Exploration Geophysics, 2013, 44: 176−184.

[87] ROUDSARI M S, BEITOLLAHI A. Laboratory modelling of self-potential anomalies due to spherical bodies [J]. Exploration Geophysics, 2015, 46: 320−331.

[88] BISWAS A. A review on modeling, inversion and

interpretation of self-potential in mineral exploration and tracing paleo-shear zones [J]. Ore Geology Reviews, 2017, 91: 21−56.

[89] MEHANEE S A. An efficient regularized inversion approach for self-potential data interpretation of ore exploration using a mix of logarithmic and non-logarithmic model parameters [J]. Ore Geology Reviews, 2014, 57: 87−115.

[90] ESSA K, MEHANEE S, SMITH P D. A new inversion algorithm for estimating the best fitting parameters of some geometrically simple body to measured self-potential anomalies [J]. Explor Geophys, 2008, 39: 155−163.

[91] MURTHY B V S, HARICHARAN P. Nomograms for the complete interpretation of spontaneous potential profiles over sheet-like and cylindrical 2D structures [J]. Geophysics, 1985, 50: 1127−1135.

[92] SUNDARARAJAN N, RAO P S, SUNITHA V. An analytical method to interpret self-potential anomalies caused by 2-D inclined sheets [J]. Geophysics, 1998, 63: 1551−1555.

[93] BISWAS A, SHARMA S P. Optimization of self-potential interpretation of 2-D inclined sheet-type structures based on very fast simulated annealing and analysis of ambiguity [J]. J Appl Geophys, 2014, 105: 235−247.

[94] DMITRIEV A N. Forward and inverse self-potential modeling: A new approach [J]. Russian Geology and Geophysics, 2012, 53(6): 611−622.

[95] BISWAS A, SHARMA S P. Resolution of multiple sheet-type structures in self-potential measurement [J]. J Earth Syst Sci, 2014, 123(4): 809−825.

[96] TIKHONOV A N, ARSENIN V Y. Solutions of ill-posed problems [M]. New York: Halsted Press, 1977.

[97] JARDANI A, REVIL A, BOLÈVE A, DUPONT J P. Three-dimensional inversion of self-potential data used to constrain the pattern of groundwater flow in geothermal fields [J]. Journal of Geophysical Research, 2008, 113: B09204.

[98] MINSLEY B J, SOGADE J, MORGAN F D. Three-dimensional source inversion of self-potential data [J]. Journal of Geophysical Research, 2007, 112: B02202.

[99] LINDE N, DOETSCH J, JOUGNOT D, GENONI O, DÜRST Y, MINSLEY B J, VOGT T, PASQUALE N, LUSTER J. Self-potential investigations of a gravel bar in a restored river corridor [J]. Hydrol Earth Syst Sci, 2011, 15: 729−742.

[100] LINDE N, REVIL A, BOLÈVE A, DAGÈS C, CASTERMANT J, SUSKI B, VOLTZ M. Estimation of the water table throughout a catchment using self-potential and piezometric data in a Bayesian framework [J]. Journal of Hydrology, 2007, 334: 88−98.

[101] ABDELRAHMAN E S M, EL-ARABY H M, HASSANEEN A R G, HAFEZ M A. New methods for shape and depth determinations from SP data [J]. Geophysics, 2003, 68(4): 1202−1210.

[102] ABDELRAHMAN E M, ESSA K S, ABO-EZZ E R, SULTAN M, SAUCK W A, GHARIEB A G. New least-squares algorithm for model parameters estimation using self-potential anomalies [J]. Comput Geosci, 2008, 34: 1569−1576.

[103] MEHANEE S A. Simultaneous joint inversion of gravity and self-potential data measured along profile: theory, numerical examples, and a case study from mineral exploration with cross validation from electromagnetic data [J]. IEEE Transactions on Geoscience and Remote Sensing, 2022, 60: 1−20.

[104] SUNGKONO, WARNANA D D. Black hole algorithm for determining model parameter in self-potential data [J]. Journal of Applied Geophysics, 2018, 148: 189−200.

[105] HARYONO A, SUNGKONO AGUSTIN R, SANTOSA B J, WIDODO A, RAMADHANY B. Model parameter estimation and its uncertainty for 2-D inclined sheet structure in self-potential data using crow search algorithm [J]. Acta Geodaetica et Geophysica, 2020, 55: 691−715.

[106] BALKAYA Ç. An implementation of differential evolution algorithm for inversion of geoelectrical data [J]. J Appl Geophys, 2013, 98: 160−175.

[107] SUNGKONO. An efficient global optimization method for self-potential data inversion using micro-differential evolution [J]. J Earth Syst Sci, 2020, 129: 178.

[108] SUNGKONO S. Robust interpretation of single and multiple self-potential anomalies via flower pollination algorithm [J]. Arabian Journal of Geosciences, 2020, 13: 100.

[109] TLAS M, ASFAHANI J. An approach for interpretation of self-potential anomalies due to simple geometrical structures using fair function minimization [J]. Pure Appl Geophys, 2013, 170: 895−905.

[110] GÖKTÜRKLER G, BALKAYA Ç. Inversion of self-potential anomalies caused by simple-geometry bodies using global optimization algorithms [J]. J Geophys Eng, 2012, 9; 498−507.

[111] DI MAIO R, RANI P, PIEGARI E, MILANO L. Self-potential data inversion through a Genetic-Price algorithm [J]. Computers & Geosciences, 2016, 94: 86−95.

[112] AGARWAL A, CHANDRA A, SHALIVAHAN S, SINGH R K. Grey wolf optimizer: A new strategy to invert geophysical data sets [J]. Geophys Prospect, 2018, 66:1215−1226.

[113] EL-KALIOUBY H M, AL-GARNI M A. Inversion of self-potential anomalies caused by 2D inclined sheets using neural networks [J]. Journal of Geophysics and Engineering, 2009, 6: 29−34.

[114] FERNANDEZ-MARTINEZ J L, GARCÍA-GONZALO E, NAUDET V. Particle swarm optimization applied to solving and appraising the streaming potential inverse problem [J]. Geophysics, 2010, 75: WA3−WA15.

[115] MONTEIRO SANTOS F A. Inversion of self-potential of idealized bodies' anomalies using particle swarm optimization [J]. Computers & Geosciences, 2010, 36: 1185−1190.

[116] LUO Y J, CUI Y A, XIE J, LU H S Z, LIU J X. Inversion of self-potential anomalies caused by simple polarized bodies based on particle swarm optimization [J]. J Cent South Univ, 2021, 28: 1797−1812.

[117] SHARMA S P, BISWAS A. Interpretation of self-potential anomaly over a 2D inclined structure using very fast simulated-annealing global optimization—An insight about ambiguity [J]. Geophysics, 2013, 78(3): WB3−WB15.

[118] BISWAS A, SHARMA S P. Interpretation of self-potential anomaly over idealized bodies and analysis of ambiguity using very fast simulated annealing global optimization

technique [J]. Near Surface Geophysics, 2015, 13(2): 179−195.

[119] ABDELAZEEM M, GOBASHY M, KHALIL M H, ABDRABOU M. A complete model parameter optimization from self-potential data using Whale algorithm [J]. Journal of Applied Geophysics, 2019, 170: 103825.

[120] BABU H V R, RAO D A. Inversion of self-potential anomalies in mineral exploration [J]. Computers & Geosciences, 1988, 14(3): 377−387.

[121] DI MAIO R, PIEGARI E, RANI P. Source depth estimation of self-potential anomalies by spectral methods [J]. J App Geophys, 2017, 136: 315−325.

[122] DI MAIO R, PIEGARI E, RANI P, AVELLA A. Self-potential data inversion through the integration of spectral analysis and tomographic approaches [J]. Geophys J Int, 2016, 206: 1204−1220.

[123] FEDI M, ABBAS M A. A fast interpretation of self-potential data using the depth from extreme points method [J]. Geophysics, 2013, 78(2): E107−E116.

[124] MURTY B V S, HARICHARAN P. SP anomaly over double line of poles-interpretation through log curves [J]. Proceedings of the Indian Academy of Sciences (Earth and Planetary Sciences), 1984, 93: 437−445.

[125] HANNINGTON M D, JONASSON I R, HERZIG P M, PETERSEN S. Physical and chemical processes of seafloor mineralization at mid-ocean ridges [M]//Seafloor Hydrothermal Systems: Physical, Chemical, Biological, and Geological Interactions. Washington: American Geophysical Union, 2013: 115−157.

[126] BOSCHEN R E, ROWDEN A A, CLARK M R, GARDNER J P A. Mining of deep-sea seafloor massive sulfides: A review of the deposits, their benthic communities, impacts from mining, regulatory frameworks and management strategies [J]. Ocean & Coastal Management, 2013, 84: 54−67.

[127] HANNINGTON M, de RONDE C, PETERSEN S. Sea-floor tectonics and submarine hydrothermal systems [C]// Economic Geology 100th Anniversary Volume. USA: Society of Economic Geologists, 2005: 111−141.

[128] FONTBOTÉ L, KOUZMANOV K, CHIARADIA M, POKROVSKI G S. Sulfide minerals in hydrothermal deposits [J]. Elements, 2017, 13: 97−103.

[129] HAN S L, ZHANG S G, LIU J X, HU H J, ZHANG W S. Integrated interpretation of dual frequency induced polarization measurement based on wavelet analysis and metal factor methods [J]. Transactions of Nonferrous Metals Society of China, 2013, 23(5): 1465−1471.

[130] LIU H F, LIU J X, GUO R W, TONG X Z, GONG L, PENG Y H. Development of multi-channel observation and inversion for IP electrical sounding method [J]. Transactions of Nonferrous Metals Society of China, 2014, 24(3): 816−823.

[131] ISHIZU K, GOTO T, OHTA Y, KASAYA T, IWAMOTO H, VACHIRATIENCHAI C, SIRIPUNVARAPORN W, TSUJI T, KUMAGAI H, KOIKE K. Internal structure of a seafloor massive sulfide deposit by electrical resistivity tomography, Okinawa trough [J]. Geophysical Research Letters, 2019, 46: 11025−11034.

[132] CAIRNS G W, EVANS R L, EDWARDS R N. A time-domain electromagnetic survey of the TAG hydrothermal mound [J]. Geophysical Research Letters, 1996, 23: 3455−3458.

[133] TAO C H, XIONG W, XI Z Z, DENG X M, XU Y X. TEM investigations of South Atlantic Ridge 13.2°S hydrothermal area [J]. Acta Oceanologica Sinica, 2013, 32: 68−74.

[134] GEHRMANN R A S, NORTH L J, GRABER S, SZITKAR F, PETERSEN S, MINSHULL T A, MURTON B J. Marine mineral exploration with controlled source electromagnetics at the TAG hydrothermal field, 26°N mid-Atlantic ridge [J]. Geophysical Research Letters, 2019, 46(11): 5808−5816.

[135] GEHRMANN R A S, HAROON A, MORTON M, DJANNI A T, MINSHULL T A. Seafloor massive sulphide exploration using deep-towed controlled source electromagnetics: Navigational uncertainties [J]. Geophysical Journal International, 2020, 220: 1215−1227.

[136] HORO D, PAL S K, AND SINGH S. Mapping of gold mineralization in Ichadih, North Singhbhum Mobile Belt, India using electrical resistivity tomography and self-potential methods [J]. Mining, Metallurgy & Exploration, 2021, 38: 397−411.

[137] ARAYA A, KANAZAWA T, SHINOHARA M, YAMADA T, FUJIMOTO H, IIZASA K, ISHIHARA T. Gravity gradiometer implemented in AUV for detection of seafloor massive sulfides [C]//2012 Oceans. VA, USA: IEEE, 2012: 1−4.

[138] SZITKAR F, PETERSEN S, CARATORI TONTINI F, COCCHI L. High-resolution magnetics reveal the deep structure of a volcanic-arc-related basalt-hosted hydrothermal site (Palinuro, Tyrrhenian Sea) [J]. Geochem Geophys Geosyst, 2015, 16: 1950−1961.

[139] HONSHO C, YAMAZAKI T, URA T, OKINO K, MOROZUMI H, UEDA S. Magnetic anomalies associated with abundant production of pyrrhotite in a sulfide deposit in the Okinawa Trough, Japan [J]. Geochem Geophys Geosyst, 2016, 17: 4413−4424.

[140] GERMAN C R, YOERGER D R, JAKUBA M, SHANK T M, LANGMUIR C H, NAKAMURA K. Hydrothermal exploration with the autonomous benthic explorer [J]. Deep Sea Research I, 2008, 55: 203−219.

[141] CORWIN R F. Offshore application of self-potential prospecting [D]. Berkeley: University of California, 1973.

[142] CHERKASHOV G A, IVANOV V N, BEL'TENEV V I, LAZAREVA L I, ROZHDESTVENSKAYA I I, SAMOVAROV M L, POROSHINA I M, SERGEEV M B, STEPANOVA T V, DOBRETSOVA I G, KUZNETSOV V Y. Massive sulfide ores of the northern equatorial Mid-Atlantic Ridge [J]. Oceanology, 2013, 53(5): 607−619.

[143] CHERKASHOV G, POROSHINA I, STEPANOVA T, IVANOV V, BEL'TENEV V E, LAZAREVA L, ROZHDESTVENSKAYA I, SAMDVAROV M, SHILOV V, GLASBY G P, FOUQUET Y, KUZNETSOV V. Seafloor massive sulfides from the northern equatorial mid-Atlantic ridge: New discoveries and perspectives [J]. Marine Georesources & Geotechnology, 2010, 28(3): 222−239.

[144] WANG J J, TAO C H, WANG H J, DENG X M, XIONG W, LI Z. Study of self-potential observation ways in the seafloor polymetallic sulfide deposits [J]. Haiyang Xuebao, 2018,

40(1): 57−67. (in Chinese).
[145] HYAKUDOME T, YOSHIDA H, ISHIBASHI S, OCHI H, SAWA T K, NAKANO Y, WATANABE Y, NAKATANI T, SUGESAWA M, OHTA Y, WATANABE K OOMIKA S, NANBU Y, KOMUKU M M. Development of AUV for scientific observation [C]//2012 Oceans. VA, USA: IEEE, 2012: 1−4.
[146] REVIL A, EHOUARNE L, THYREAULT E. Tomography of self-potential anomalies of electrochemical nature [J]. Geophysical Research Letters, 2001, 28(23): 4363−4366.
[147] YEATS C J, HOLLIS S P, HALFPENNY A, CORONA J C, LAFLAMME C, SOUTHAM G, FIORENTINI M, HERRINGTON R J, SPRATT J. Actively forming Kuroko-type volcanic-hosted massive sulfide (VHMS) mineralization at Iheya North, Okinawa Trough, Japan [J]. Ore Geology Reviews, 2017, 84: 20−41.
[148] YAMAMOTO M, NAKAMURA R, KASAYA T, KUMAGAI H, SUZUKI K, KEN T K. Spontaneous and widespread electricity generation in natural deep-sea hydrothermal fields [J]. Angew Chem (Int Ed), 2017, 56: 5725−5728.
[149] LIAO S L, TAO C H, LI H M, BARRIGA F J A S, LIANG J, YANG W F, YU J Y, ZHU C W. Bulk geochemistry, sulfur isotope characteristics of the Yuhuang-1 hydrothermal field on the ultraslow-spreading Southwest Indian Ridge [J]. Ore Geology Reviews, 2018, 96: 13−27.
[150] REVIL A, KARAOULIS M, JOHNSON T, KEMNA A. Review: Some low-frequency electrical methods for subsurface characterization and monitoring in hydrogeology [J]. Hydrogeology Journal, 2012, 20(4): 617−658.
[151] HÖRDT A, BAIRLEIN K, SPAGNOLI G, JEGEN M, HANNINGTON M, PETERSEN S, LAURILA T E. Induced polarization of seafloor massive sulfides [C]//International workshop on induced polarization. Aarhus, Denmark: University of Aarhus, 2016. doi.org/10.1016/j.cageo.2015.09.015.

自然电位法在海洋矿产勘探中的理论、正反演计算及应用进展

谢 静[1,2,3]，崔益安[1,2,3]，柳建新[1,2,3]，郭友军[1,2,3]，张丽娟[1,2,3]，罗议建[1,2,3]，张鹏飞[1,2,3]

1. 中南大学 地球科学与信息物理学院，长沙 410083；
2. 湖南省有色资源与地质灾害探查湖南省重点实验室，长沙 410083；
3. 中南大学 有色金属成矿预测与地质环境监测教育部重点实验室，长沙 410083

摘 要：自然电位法是一种被动地球物理勘探方法，其通过在地表、井中或(海)水中测量由电化学、电动和热电机制引发的自然电位异常进而开展相关勘探工作。自然电位法与地下水流及(电)化学梯度有直接关联，已在矿产勘探、环境调查以及水文地球物理问题中受到越来越多的关注和应用。本文主要回顾自然电位法在矿产勘探领域的源机制、数值模拟和反演解释理论，以及该方法在矿产勘探中的应用。同时，总结 3 个海底硫化物矿床勘探案例，以说明自然电位法在海洋矿产勘探中的特点及应用效果。本研究对探讨自然电位法在深海找矿中的应用具有重要意义。

关键词：自然电位；海洋矿产勘探；源机制；数值模拟；反演解释

(Edited by Xiang-qun LI)